Supporting Information

Supramolecularly Modulated Carbon-Centered Radicals: Toward Selective Oxidation from Benzyl Alcohol to Aldehyde

Xingchen Tang, Shan Mei, Jiang-Fei Xu*, Xi Zhang

Department of Chemistry, Tsinghua University
Email: xujf@mail.tsinghua.edu.cn

1. Instrumentations and methods

All chemical materials and solvents were procured from commercial suppliers and utilized without the need for additional purification. Cucurbit[7]uril (CB[7]) was synthesized in accordance with previously published literature.[1]

The ^{1}H NMR spectra and ^{13}C NMR were acquired using a JOEL JNM-ECZ400S/L1 spectrometer operating at 400 MHz. ESI-MS spectra were recorded on a SHIMADZU LCMS-IT/TOF system with acetonitrile/water serving as the mobile phase. Isothermal titration calorimetry (ITC) experiments were executed using a Microcal VP-ITC calorimeter in a phosphate buffer solution with varying pH levels at a consistent temperature of 25 °C. UV-Vis spectra were captured via a HITACHI UH4150 spectrophotometer. Electronic paramagnetic resonance (EPR) measurements were performed on a JEOL JES-FA200 apparatus, utilizing a 9426 MHz microwave frequency and 0.9980 mW power. Electrochemical measurements were conducted with an Autolab electrochemical workstation (PGSTAT12) employing a three-electrode system. pH values were determined, and pH titrations were carried out at 25 °C using a Mettler Toledo S210 pH meter equipped with a Mettler Toledo Inlab Micro electrode. Photolysis reactions were conducted using a 3S-Tech AS-1-U photoreactor equipped with a 308 nm LED light source, both procured from Shanghai 3S Technology Co., Ltd. The LED emitted light with a peak at 308 nm and a full width at half maximum (FWHM) of 10 nm. The power of the LED was maintained at 3.00 W, with optical power density of 1.207 mW/cm^2.
EPR measurements were performed using the samples sealed in glass capillaries with LED light irradiated in situ. Spectrolelectrochemical experiments were conducted using a quartz cuvette with 1.0 mm optical length. Compound was dissolved in 0.1 M saline electrolyte with concentration of 40 μM. Absorption signal as recorded simultaneously upon applying constant voltage, where a platinum net, a platinum wire was used as working electrode and counter electrode respectively, with a silver chloride reference

electrode.

Photolysis reactions were performed in a 20 mM phosphate buffer D_2O solution to maintain a stable pD value during carboxylic product generation. A quartz cuvette was employed as the reaction container to ensure optimal UV light transmission. The quartz cuvette contained a magnetic bar and was positioned 1.0 cm from the LED source, with one face oriented toward the light. Substrates were fixed at a concentration of 2.0 mM, while the CB[7] concentration varied as indicated. The reaction solution volume was standardized to 0.60 mL. Photolysis reactions were carried out using an LED light source, and conversion of the photolysis reactions was determined through NMR integrals.

Aldehyde selectivity was defined as $Selectivity = \frac{n(Aldehyde)t}{n(Alcohol)0 - n(Alcohol)t}$.

$n(Alcohol)_0$ means the initial amount of benzyl alcohol and $n(Alcohol)_t$ means the amount of benzyl alcohol when the reaction time is t.

2. Synthesis and characterization

1) Synthesis of compound PAL and PAL-Cl

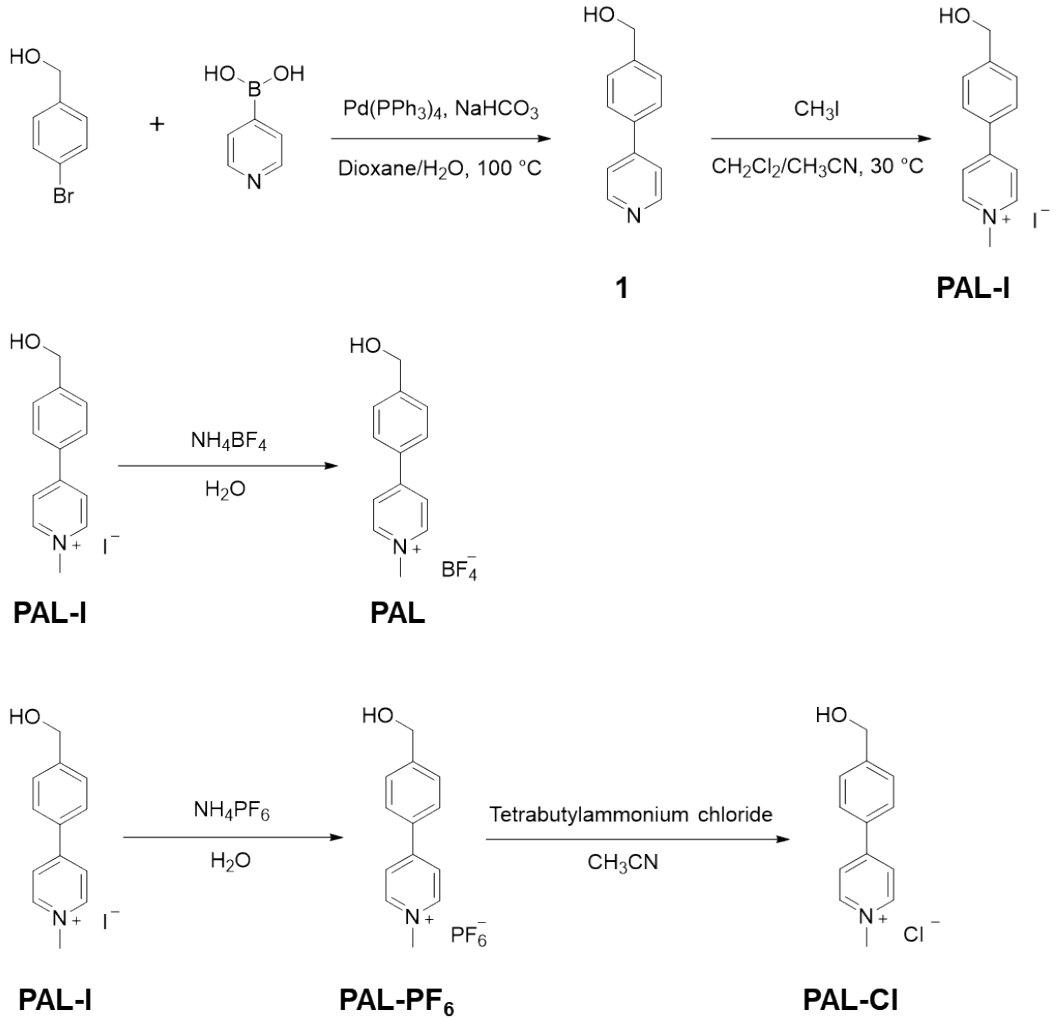

Figure S1. Synthetic route of PAL and PAL-Cl.

Compound 1: 4-Bromobenzyl alcohol (561 mg, 3.00 mmol), 4-Pyridinylboronic acid (554 mg, 4.50 mmol), $Pd(PPh_3)_4$ (34.0 mg, 0.0300 mmol), and sodium bicarbonate (1.13 g, 13.5 mmol) were dissolved in a mixture of dioxane and water (3:2, v/v). The solution was subjected to a 10-minute purge with N_2 and was subsequently stirred at 90 °C in an oil bath overnight. After cooling to room temperature, additional water was added, and the solution was subjected to three extractions with ethyl acetate. The organic phase was dried with anhydrous sodium sulfate for 2 hours. The product was purified by silica gel column chromatography, utilizing petroleum ether and ethyl acetate eluent (1:1, v/v), yielding a white solid (472 mg, 85% yield). ^{1}H NMR ($CDCl_3$, 400 MHz): δ[ppm] = 8.66 (d, J = 5.2 Hz, 2H), 7.65 (d, J = 7.8 Hz, 2H), 7.51 (m, 4H), 4.78 (d, J = 4.8 Hz, 2H), 1.81 (t, J = 5.9 Hz, 1H). HRMS (ESI) m/z : $[M + H]^+$ calculated for $C_{12}H_{13}NO^+$, 186.0913; found 186.0911.

Compound PAL-I: Compound 1 (500 mg, 2.70 mmol) and iodomethane (1.92 g, 13.5 mmol) was added to 30 mL mixture of dichloromethane and acetonitrile (1:1, v/v), and stirred at 30 °C in an oil bath overnight. 30 mL diethyl ether was added to precipitate the product. The precipitate was filtered and washed to give a pale-yellow solid (866 mg, 98% yield). ^{1}H NMR (DMSO-d_6, 400 MHz): δ[ppm] = 8.99 (d, *J* = 6.6 Hz, 2H), 8.50 (d, *J* = 7.0 Hz, 2H), 8.06 (d, *J* = 8.4 Hz, 2H), 7.57 (d, *J* = 8.2 Hz, 2H), 5.41 (t, *J* = 5.7 Hz, 1H), 4.62 (d, *J* = 5.7 Hz, 2H), 4.32 (s, 3H).

Compound PAL: Compound PAL-I (327 mg, 1.00 mmol) was dissolved in water to a saturated concentration. Ammonium tetrafluoroborate (318 mg, 3.06 mmol) was dissolved in water to saturation and added to the aqueous solution of PAL-I under stirring. The mixture was cooled at 4 °C overnight and the precipitate was filtered and washed to give a white solid (280 mg, 98% yield). ^{1}H NMR (DMSO-d_6, 400 MHz): δ[ppm] = 8.97 (d, *J* = 6.9 Hz, 2H), 8.49 (d, *J* = 7.0 Hz, 2H), 8.06 (d, *J* = 8.3 Hz, 2H), 7.57 (d, *J* = 8.2 Hz, 2H), 5.40 (s, 1H), 4.62 (s, 2H), 4.31 (s, 3H). HRMS (ESI) m/z : $[M]^+$ calculated for $C_{13}H_{14}NO^+$, 200.1070; found 200.1070.

Compound PAL-PF_6: Compound PAL-I (327 mg, 1.00 mmol) was dissolved in water to a saturated concentration. Ammonium hexafluorophosphate (499 mg, 3.06 mmol) was dissolved in water to saturation and added to the aqueous solution of PAH-I under stirring. The mixture was cooled at 4 °C overnight and the precipitate was filtered and washed to give a white solid (335 mg, 97% yield). ^{1}H NMR (DMSO-d_6, 400 MHz): δ[ppm] = 8.99 (d, *J* = 6.8 Hz, 2H), 8.49 (d, *J* = 7.0 Hz, 2H), 8.06 (d, *J* = 8.4 Hz, 2H), 7.57 (d, *J* = 8.1 Hz, 2H), 5.43 (t, *J* = 5.6 Hz, 1H), 4.62 (d, *J* = 5.6 Hz, 2H), 4.32 (s, 3H).

Compound PAL-Cl: Compound PAL-PF_6 (345 mg, 1.00 mmol) was dissolved in acetonitrile to a saturated concentration. Tetrabutylammonium chloride (850 mg, 3.06 mmol) was dissolved in acetonitrile to saturation and added to the solution of PAL-PF_6 under stirring. The mixture was cooled at 4 °C overnight and the precipitate was filtered and washed to give a white solid (220 mg, 94% yield). ^{1}H NMR (DMSO-d_6, 400 MHz): δ[ppm] = 8.99 (d, *J* = 6.8 Hz, 2H), 8.49 (d, *J* = 7.0 Hz, 2H), 8.06 (d, *J* = 8.4 Hz, 2H), 7.57 (d, *J* = 8.1 Hz, 2H), 5.43 (t, *J* = 5.6 Hz, 1H), 4.62 (d, *J* = 5.6 Hz, 2H), 4.32 (s, 3H). HRMS (ESI) m/z : $[M]^+$ calculated for $C_{13}H_{14}NO^+$, 200.1070; found 200.1075.

2) Synthesis of compound PCA and PCA-Cl

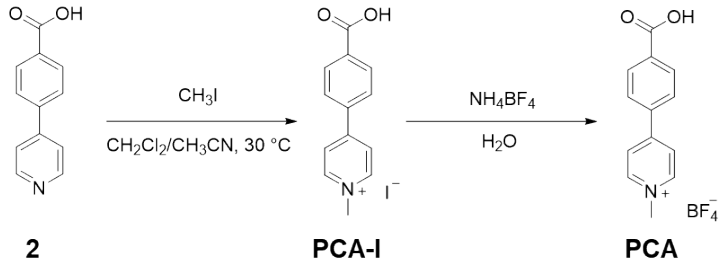

Figure S2. Synthetic route of PCA.

Compound PCA-I: Compound 2 (500 mg, 2.51 mmol) and iodomethane (1.92 g, 13.5 mmol) was added to 30 mL mixture of dichloromethane and acetonitrile (1:1, v/v), and stirred at 30 °C in an oil bath for 72 hours. Over this period, the initial white suspension gradually transitioned to a yellowish color. The resulting solid was filtered and washed. After recrystallization and overnight drying, a yellow solid was obtained (866 mg, 98% yield). ^{1}H NMR (DMSO-d_6, 400 MHz): δ[ppm] = 13.36 (s, 1H), 9.07 (d, J = 6.5 Hz, 2H), 8.55 (d, J = 6.7 Hz, 2H), 8.23 – 8.11 (m, 4H), 4.35 (s, 3H).

Compound PCA: Compound PCA-I (209 mg, 0.612 mmol) was dissolved in water to a saturated concentration. Ammonium tetrafluoroborate (318 mg, 3.06 mmol) was dissolved in water to saturation. This solution was added to the aqueous solution of Compound PCA-I under stirring. The resulting mixture was cooled to 4 °C overnight. Subsequently, the precipitate was filtered and washed to yield a white solid. (174 mg, 95%). ^{1}H NMR (DMSO-d_6, 400 MHz): δ[ppm] = 13.31 (s, 1H), 9.07 (d, J = 7.0 Hz, 2H), 8.56 (d, J = 7.0 Hz, 2H), 8.28 – 8.09 (m, 4H), 4.36 (s, 3H).

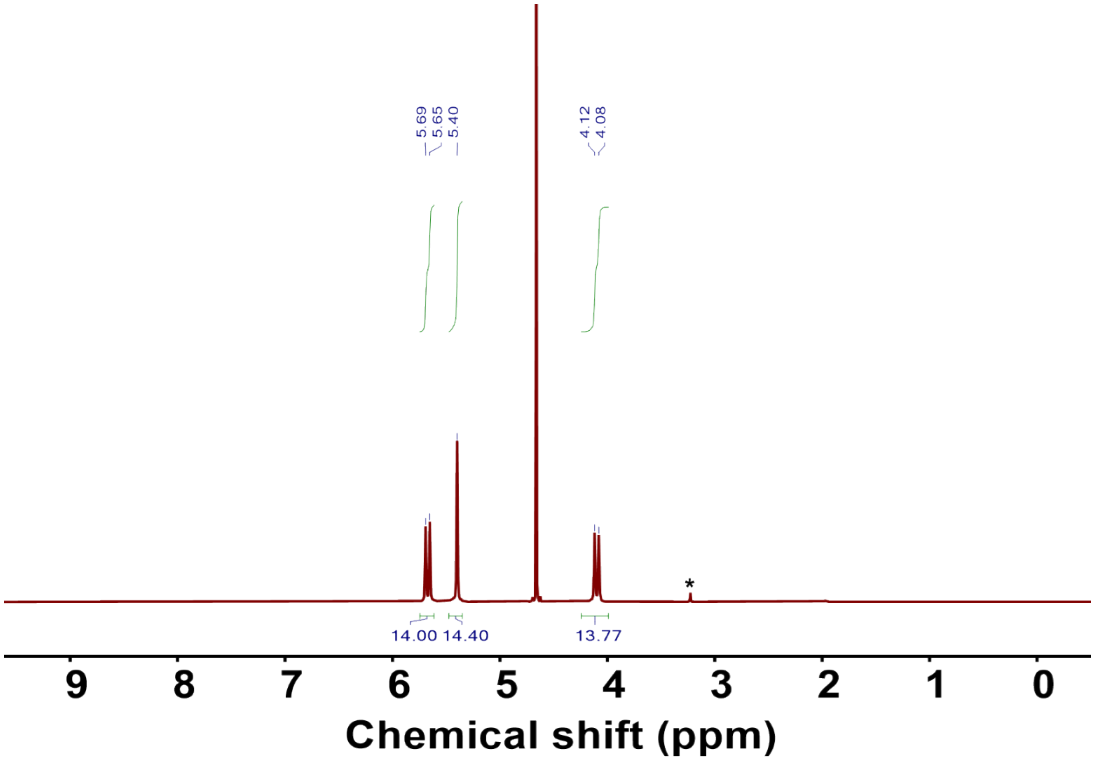

Figure S3. ^{1}H NMR of CB[7] in D2O.

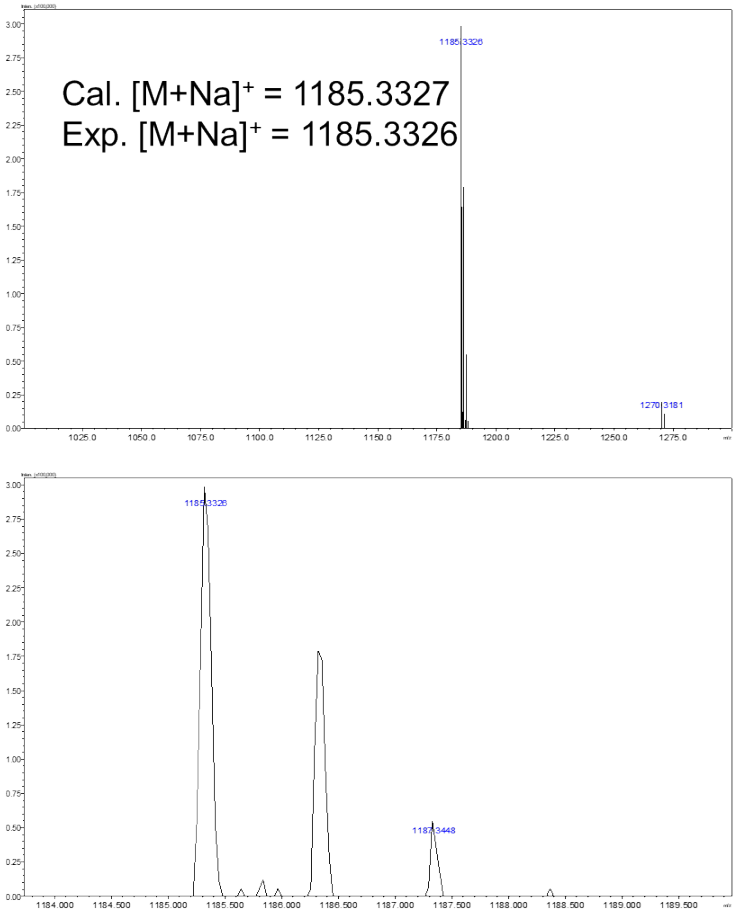

Figure S4. ESI-MS spectra of CB[7].

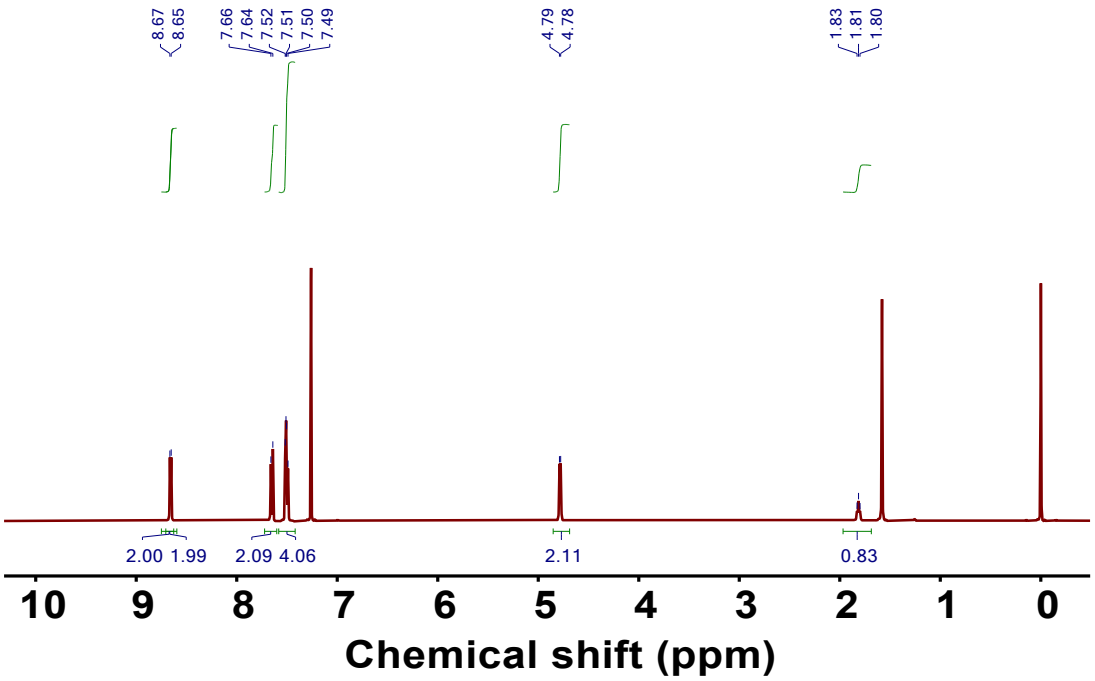

Figure S5. ^{1}H NMR of 1 in $CDCl_3$.

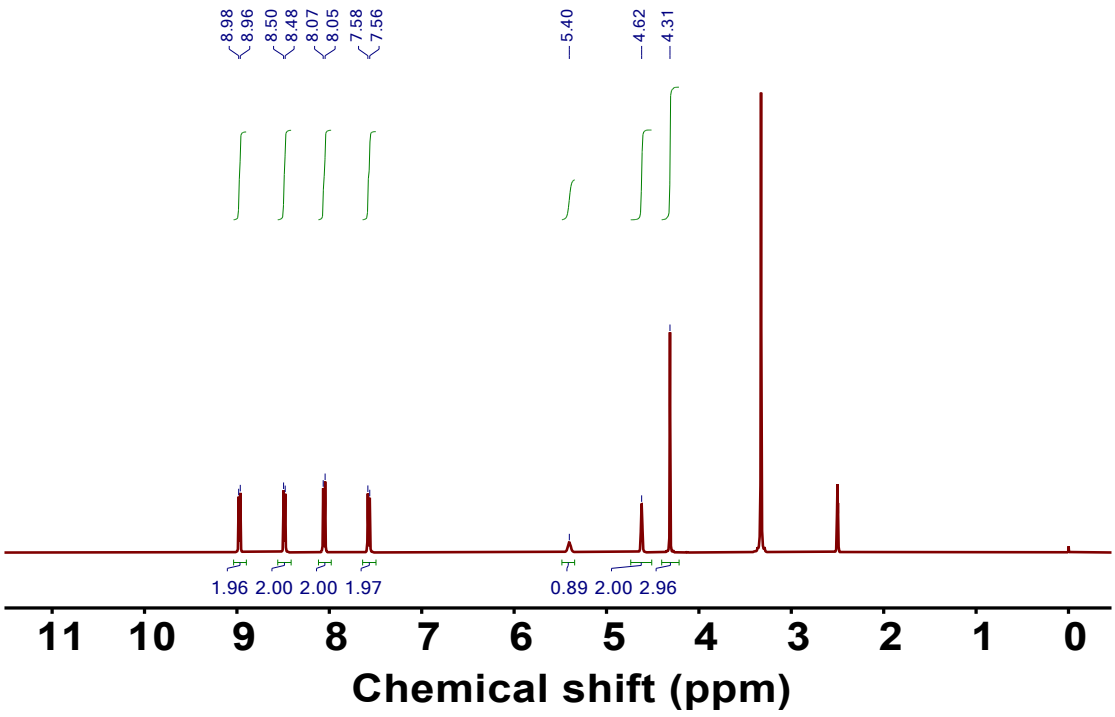

Figure S6. ^{1}H NMR of PAL in DMSO-d_6.

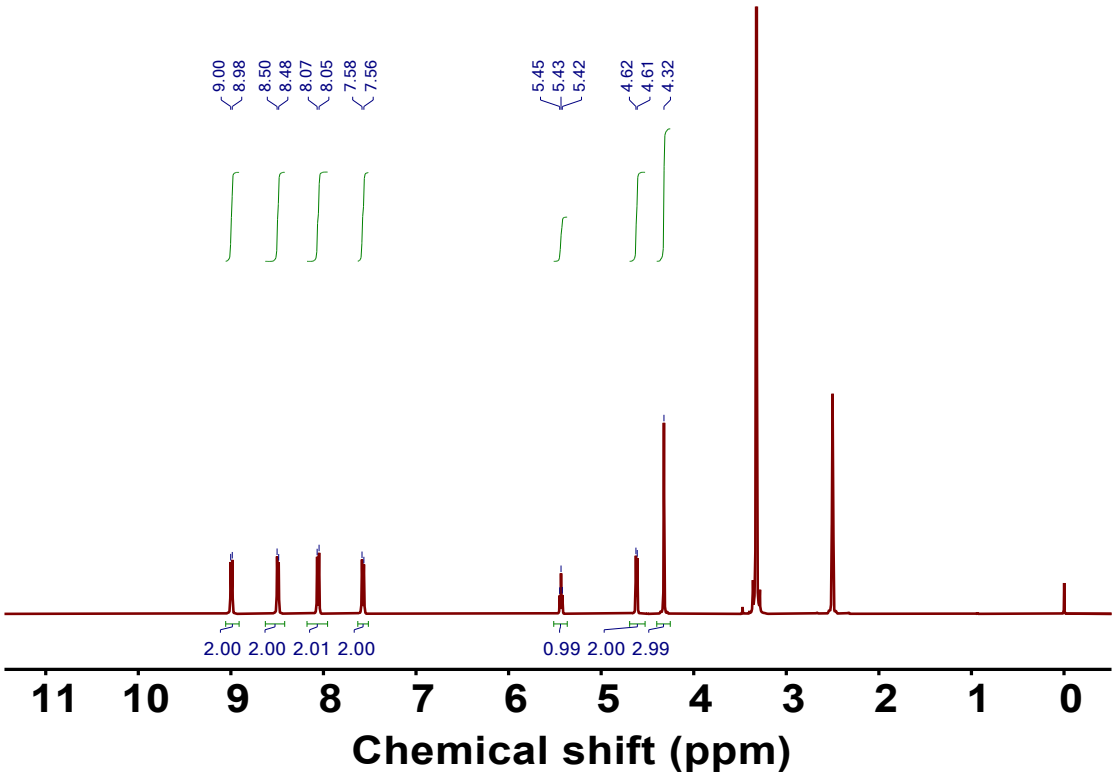

Figure S7. ^{1}H NMR of PAL-Cl in DMSO-d_6.

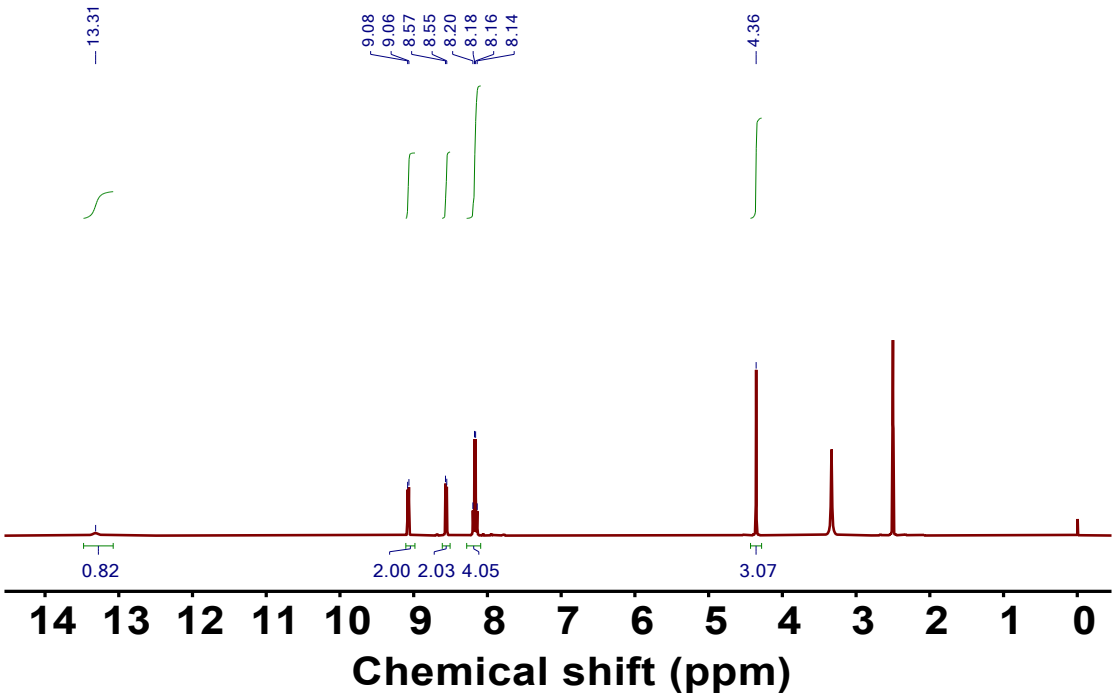

Figure S8. ^{1}H NMR of PCA in DMSO-d_6.

3. UV/Vis spectra of PAL and PAL/CB[7]

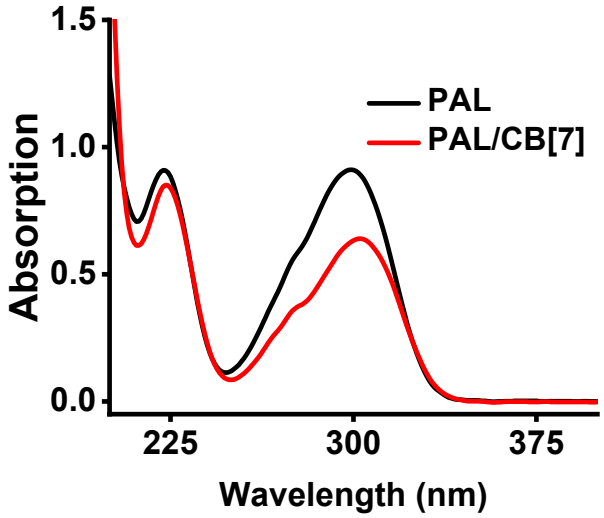

Figure S9. UV/Vis spectra of PAL and PAL/CB[7] (40 μM in water).

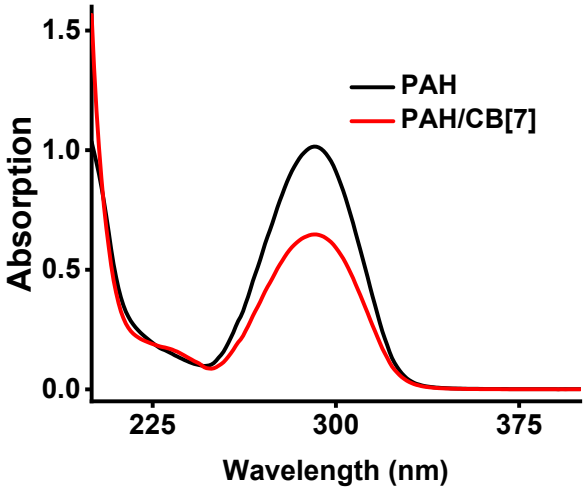

Figure S10. UV/Vis spectra of PAH and PAH/CB[7] (40 μM in water).

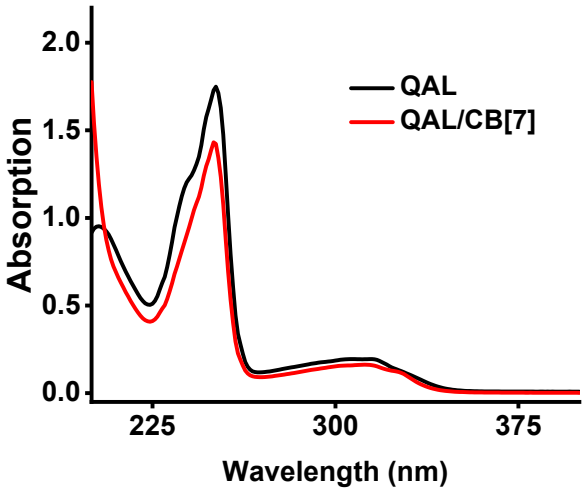

Figure S11. UV/Vis spectra of QAL and QAL/CB[7] (40 μM in water).

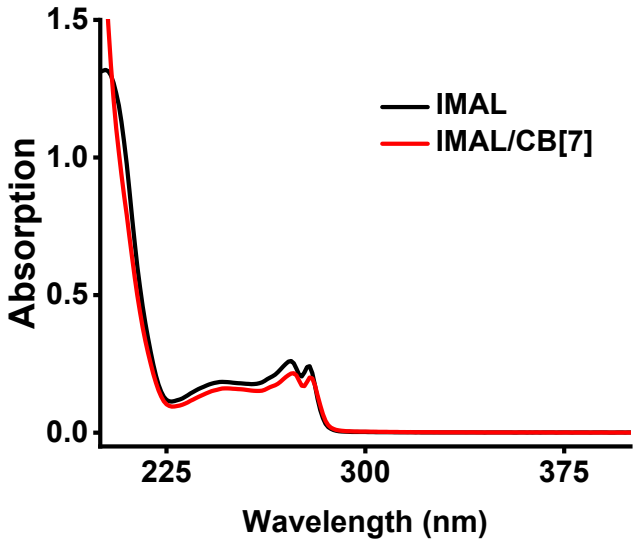

Figure S12. UV/Vis spectra of IMAL and IMAL/CB[7] (40 μM in water).

4. Complexation of compound PAH, and PCA with CB[7]

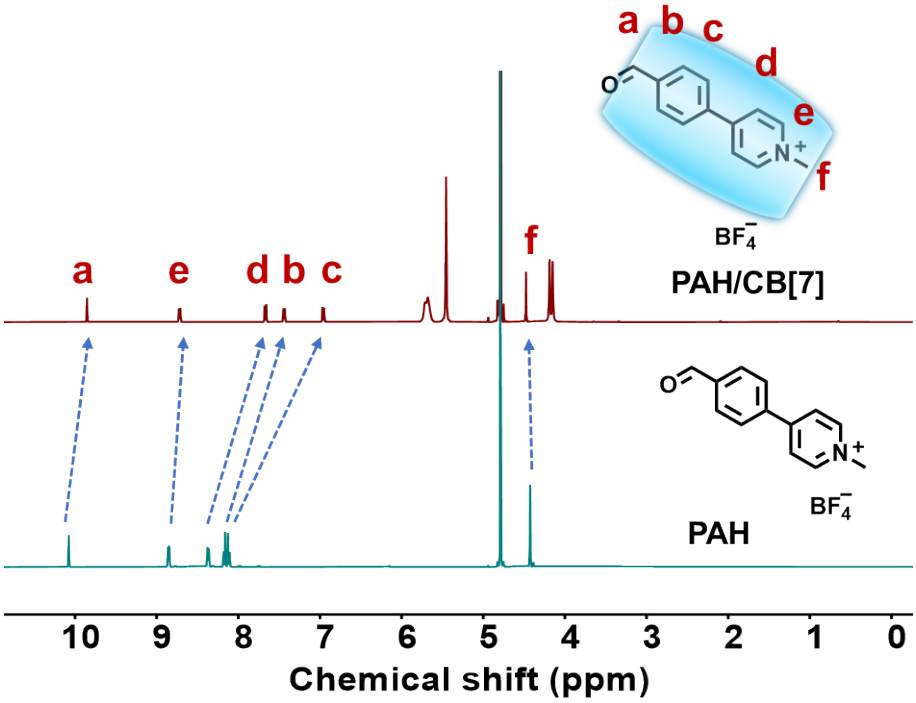

Figure S13. ^{1}H NMR of PAH and corresponding complexation with CB[7] in D_2O (pD = 7.4, phosphate buffer).

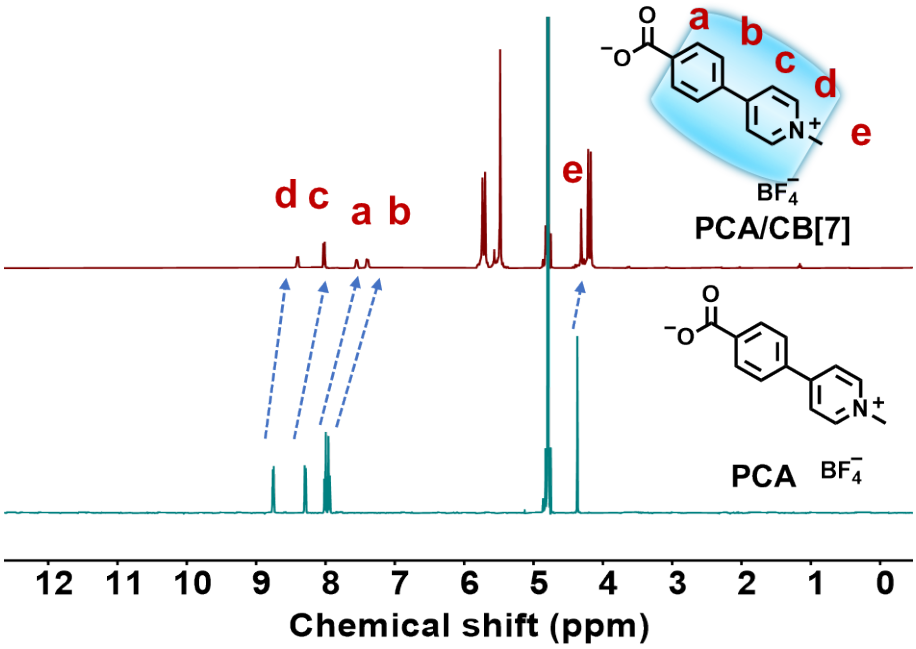

Figure S14. ^{1}H NMR of PCA and corresponding complexation with CB[7] in D_2O (pD = 7.4, phosphate buffer).

5. Complexation of compound QAL, and IMAL with CB[7]

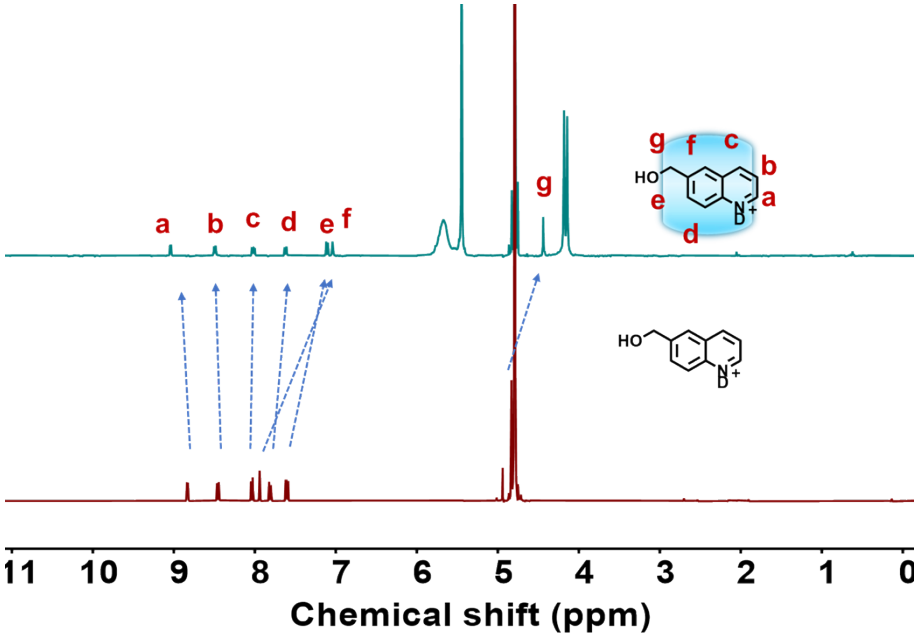

Figure S15. ^{1}H NMR of QAL and corresponding complexation with CB[7] in D_2O (pD = 2.0, phosphate buffer).

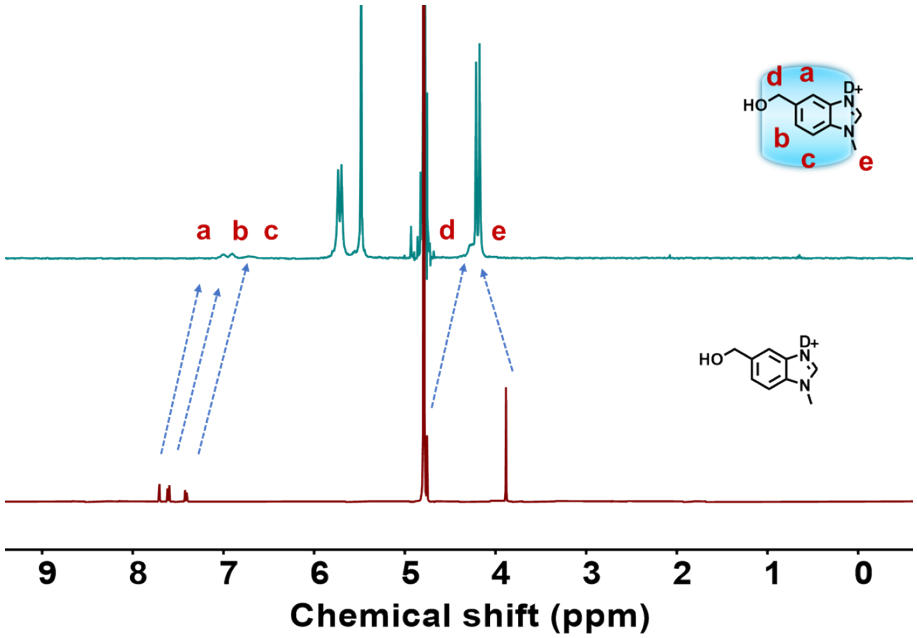

Figure S16. ^{1}H NMR of IMAL and corresponding complexation with CB[7] in D_2O (pD = 2.0, phosphate buffer).

6. The influence of pH

Photo-induced oxidation reactions were carried out in acid/alkaline (pD = 2.0/pD = 10.3) phosphate buffers, respectively. As shown in Figure S17, when PAL/CB[7] was irradiated in an acidic buffer with pD 2.0 for 10 h, the yield of PAH/CB[7] was 86%. The aldehyde selectivity was 91%, which was significantly higher than the control group without CB[7] (< 41% aldehyde selectivity). In the case of the alkaline buffer with pD 10.3, PAL/CB[7] was completely consumed after 10 h of irradiation, affording the yield and selectivity of aldehyde as high as 88% and 97%. As the control, irradiating PAL in alkaline buffer only afforded the aldehyde selectivity no higher than 48%. Therefore, the host-guest interaction of CB[7] contributes to the remarkably high aldehyde yield and selectivity of photo-induced oxidation of benzyl alcohol in a wide range of pH values.

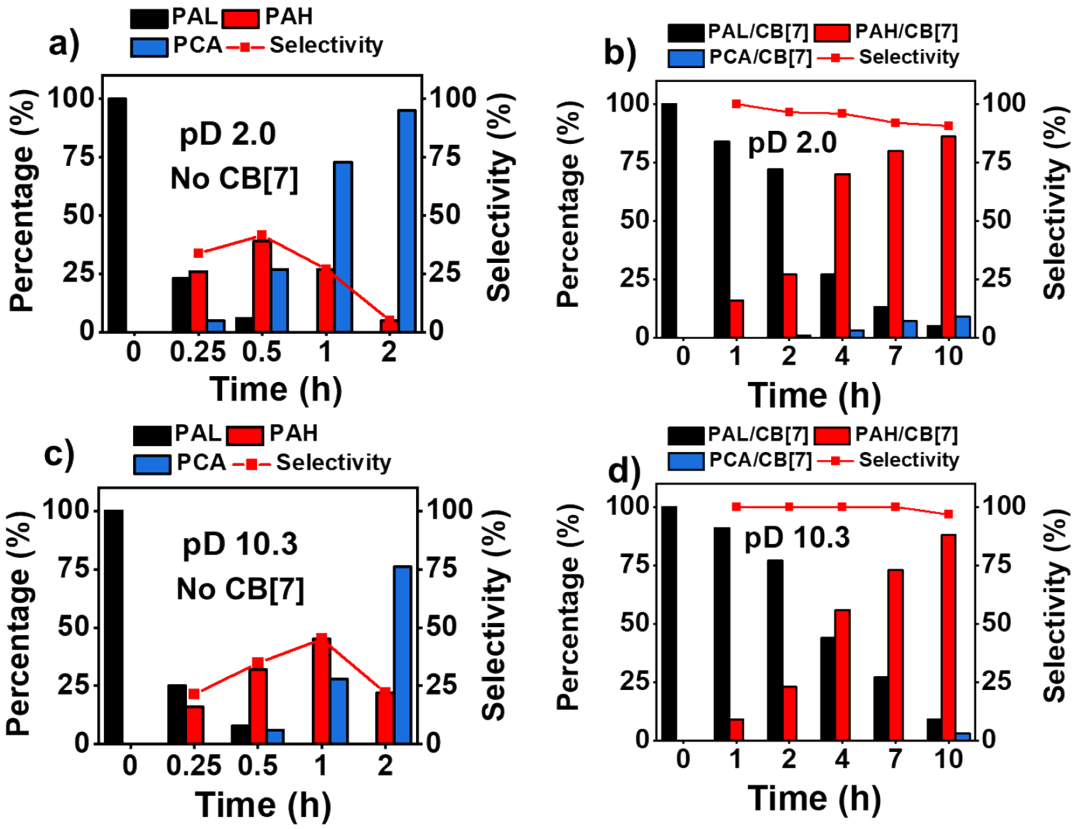

Figure S17. a) Kinetic profile of photo-induced oxidation of PAL in pD = 2.0 buffer in the absence or b) in the presence of CB[7]. c) The above reaction in pD = 10.3 buffer in the absence or d) in the presence of CB[7].

7. The influence of iodide ion

To investigate the influence of iodide ion on the reaction, photo-oxidation reactions were performed using PAL-I and PAL-I/CB[7] as substrates. As shown in Figure S18, the photo-oxidation of PAL-I was a bit slower than PAL, and large amount of carboxylic acid emerged when the reaction was extended to 10 h. The yield and selectivity of aldehyde remained no higher than 65%. In stark contrast, high aldehyde yield (90%) and selectivity (92%) could be observed for the host-guest complex of PAL-I/CB[7]. These result shows that this supramolecular strategy exhibits tolerance to iodide ion.

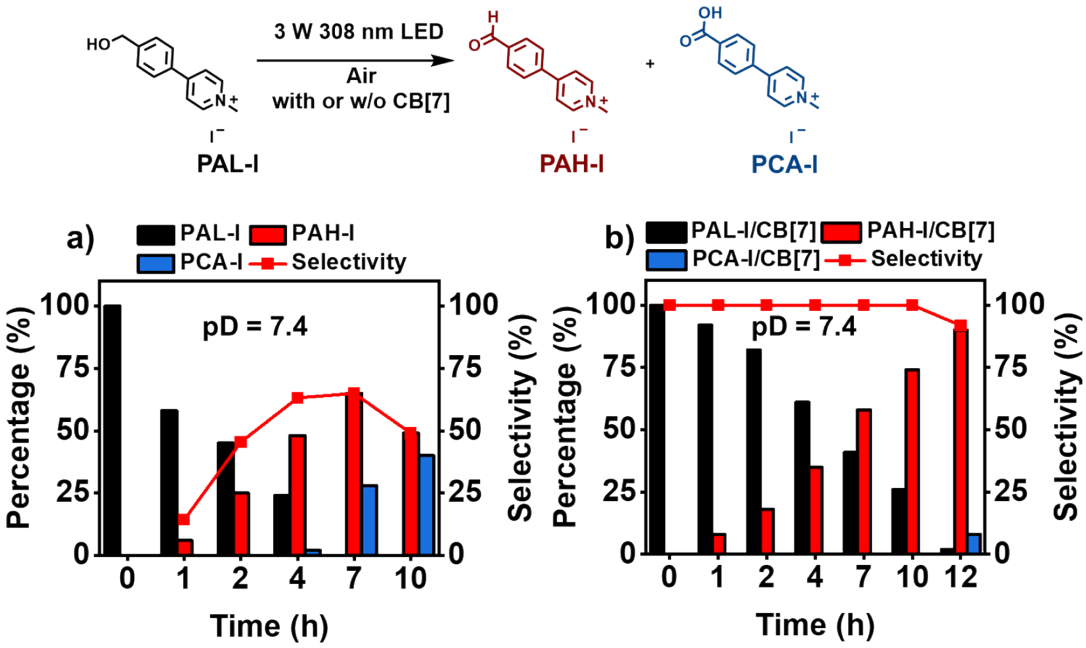

Figure S18. Kinetic profile of photo-induced oxidation of PAL-I in pD = 7.4 buffer in the absence or c) in the presence of CB[7].

8. The influence of chloride ion

To investigate the influence of chloride ion on the reaction, photo-oxidation reactions were performed using PAL-Cl and PAL-Cl/CB[7] as substrates. As shown in Figure S20-S22, a similar enhancement of aldehyde selectivity could also be observed for the host-guest complex of PAL-Cl/CB[7] in pD ranging from 2.0 to 10.3.

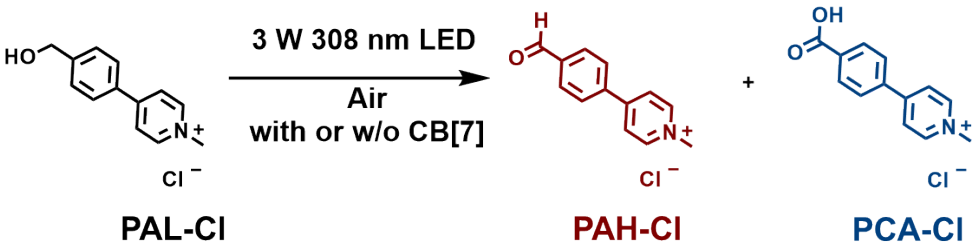

Figure S19. Photo-induced oxidation of PAL to PAH or PCA with or without CB[7].

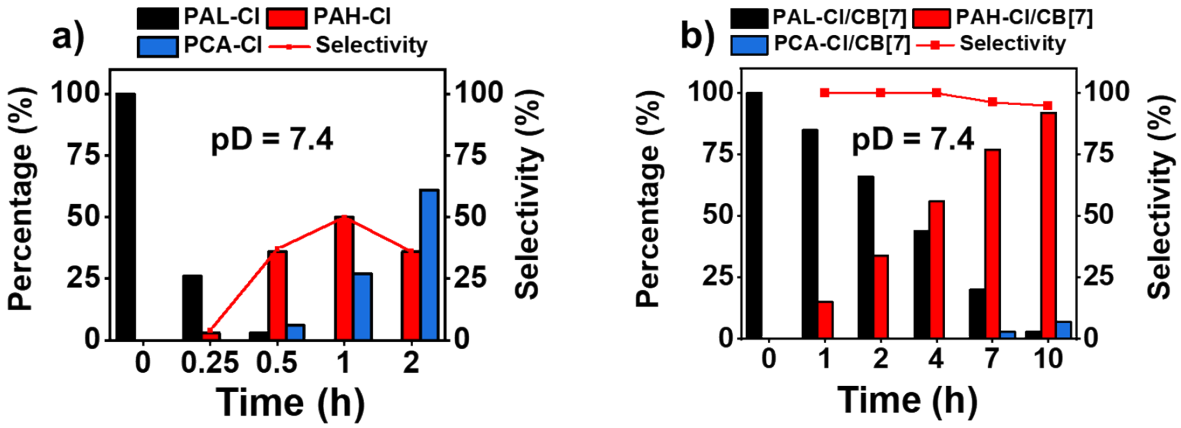

Figure S20. Kinetic profile of photo-induced oxidation of PAL-Cl in pD = 7.4 buffer in the absence or c) in the presence of CB[7].

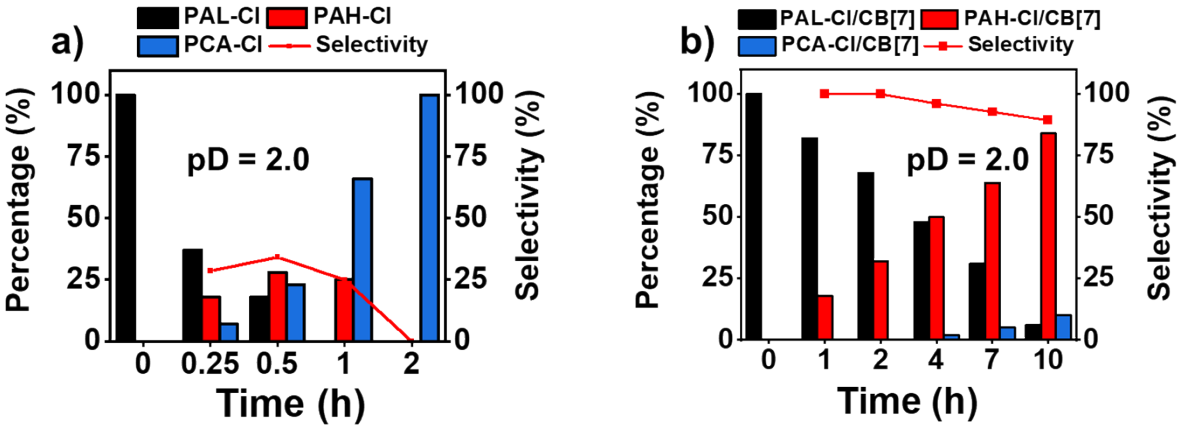

Figure S21. Kinetic profile of photo-induced oxidation of PAL-Cl in pD = 2.0 buffer in the absence or c) in the presence of CB[7].

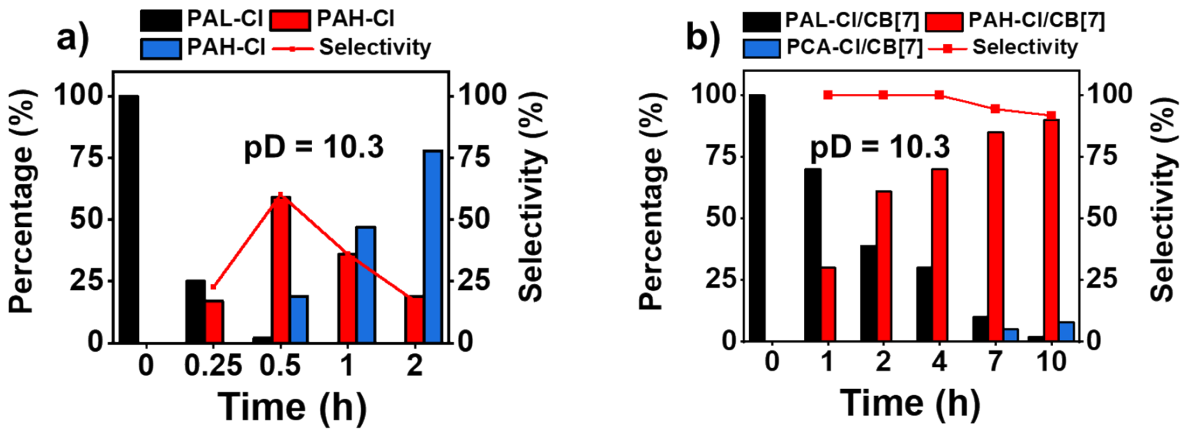

Figure S22. Kinetic profile of photo-induced oxidation of PAL-Cl in pD = 10.3 buffer in the absence or c) in the presence of CB[7].

9. The influence of CB[7] stoichiometry

To test the stoichiometry of CB[7] on the enhancement of aldehyde selectivity, different amount of CB[7] were added to PAL and then irradiated respectively in pD 7.4. As shown in Figure S23, when 0.8 eq CB[7] was added, the yield of PAH reached its maximum of about 55% within the first hour and gradually decreased, while the highest selectivity was 71%. When 1.2 eq CB[7] was added, high aldehyde selectivity of about 100% was observed when irradiated for 10 h, which was slightly higher than the case of 1.0 eq CB[7] added. Therefore, 1.0 eq CB[7] is required and sufficient to improve the selectivity of photo-induced oxidation reaction to yield benzyl aldehyde.

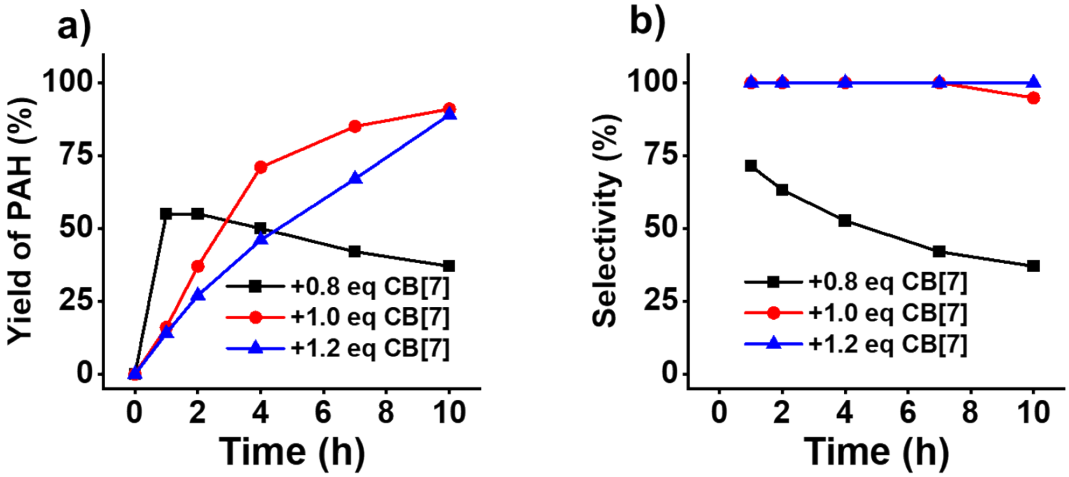

Figure S23. Time-aldehyde selectivity of the photo-induced oxidation of PAL with different ratios of CB[7].

10. Byproduct analysis

The generated ketyl radical underwent rapid dimerization to yield large amount of pinacol-type byproduct during the early phase of the reaction, as shown in Figure S24-S27. The host-guest interaction of CB[7] significantly inhibited the production of the byproduct.

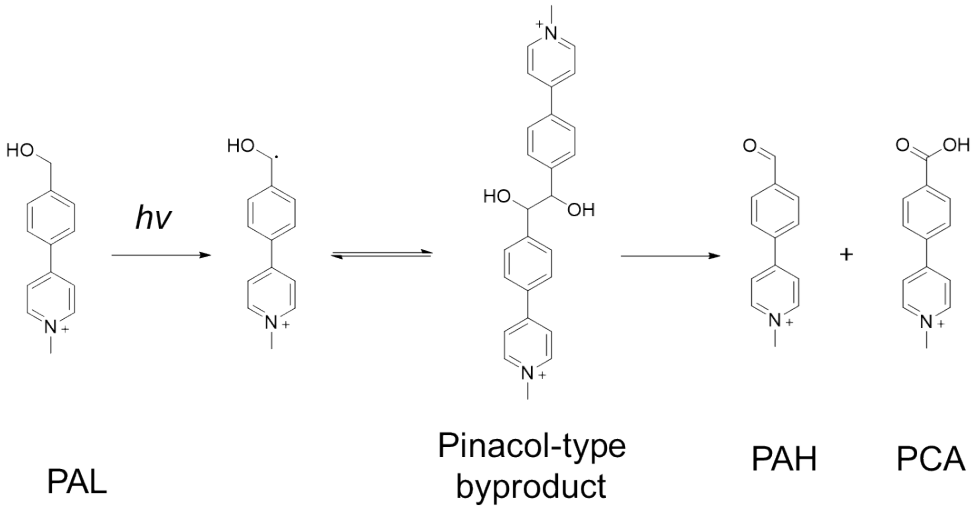

Figure S24. Illustration of the formation and consumption of the pinacol type byproduct by irradiating PAL in the absence of CB[7].

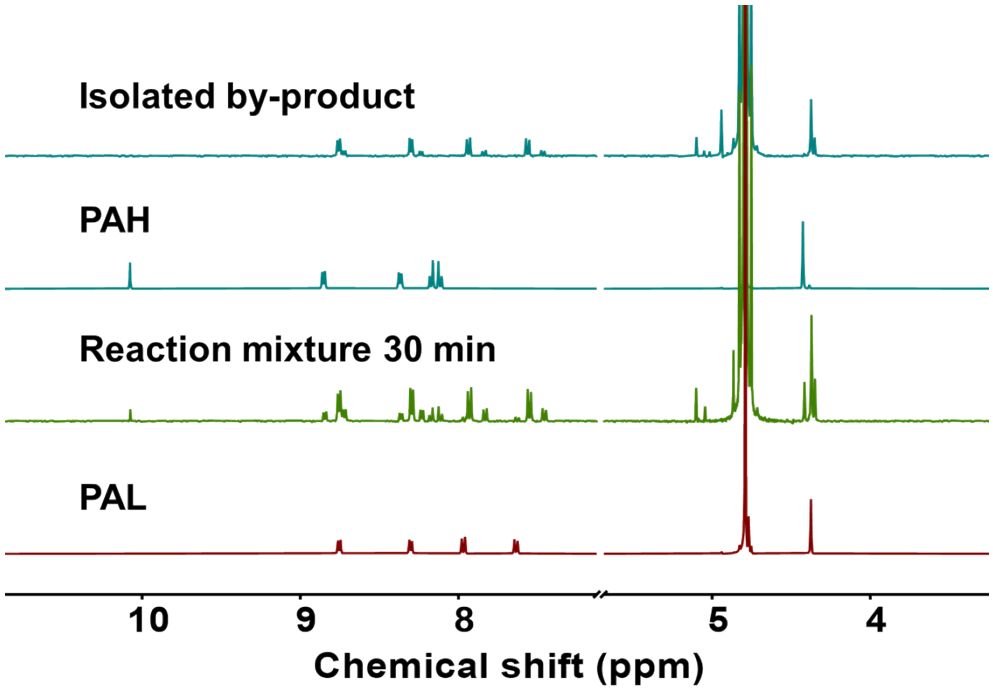

Figure S25. ^{1}H NMR spectra of compound PAL, reaction mixture after irradiating for 30 min, compound PAH and pinacol-type byproduct isolated from reaction mixture.

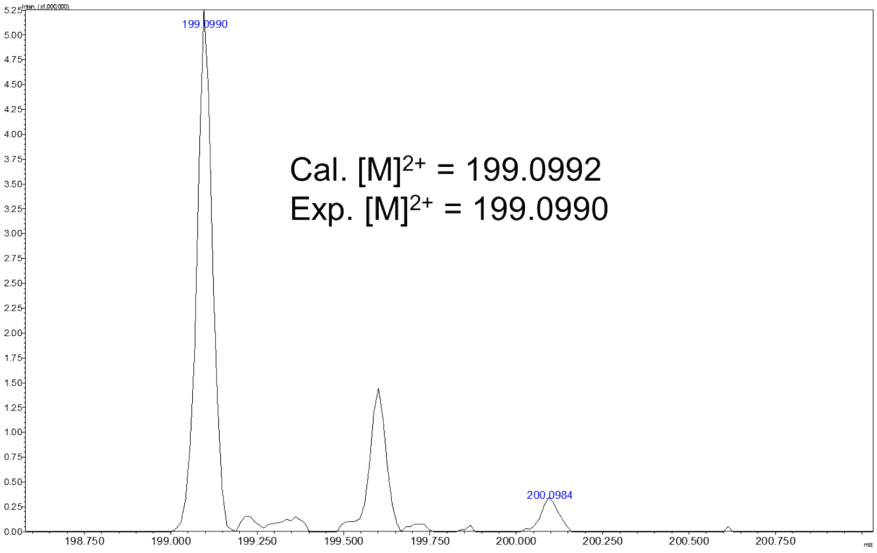

Figure S26. ESI-MS spectrum of isolated pinacol-type byproduct.

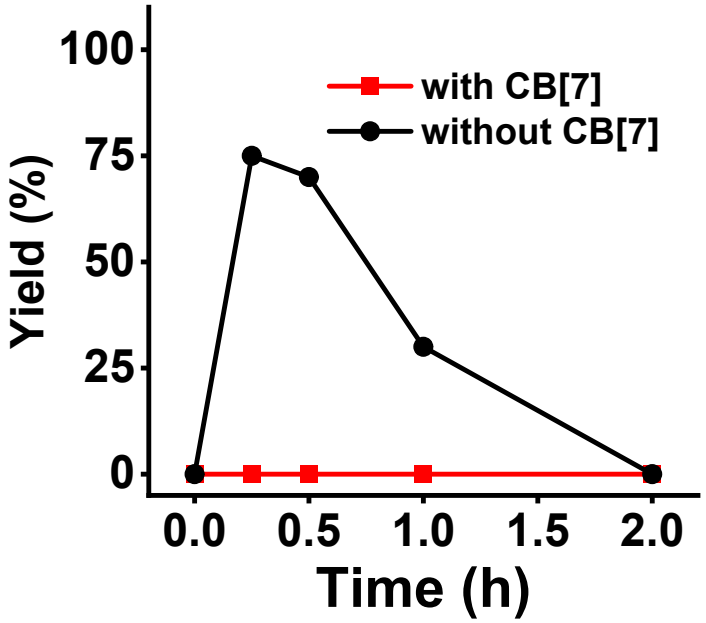

Figure S27. The yield of pinacol-type byproduct in the absence and presence of CB[7]. The yields of pinacol were determined by ^{1}H NMR.

11. Photo-oxidation of QAL and IMAL

Reactions were carried out using the same apparatus described in above sections. Phosphate buffer of pD 2.0 was chosen as reaction medium, in which QAL and IMAL can be protonated and tend to form stable host-guest complexed with CB[7].

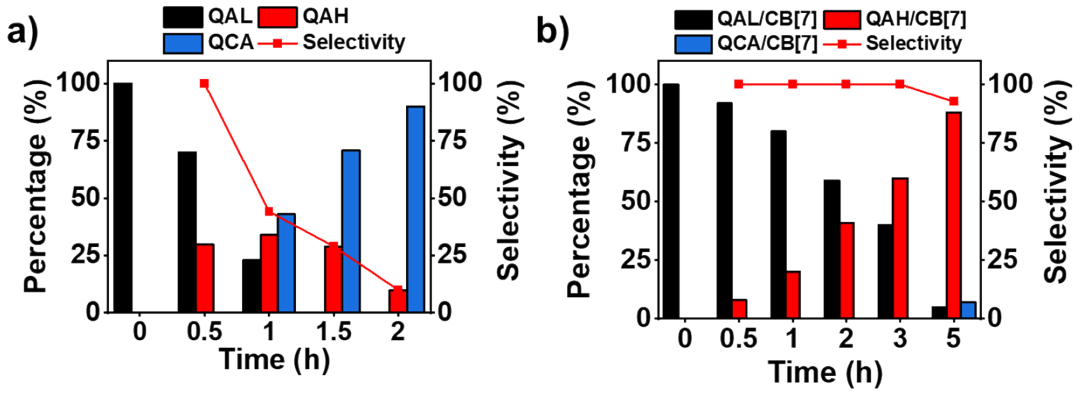

Figure S28. Kinetic profile of photo-induced oxidation of QAL in pD 2.0 buffer in the absence or c) in the presence of CB[7].

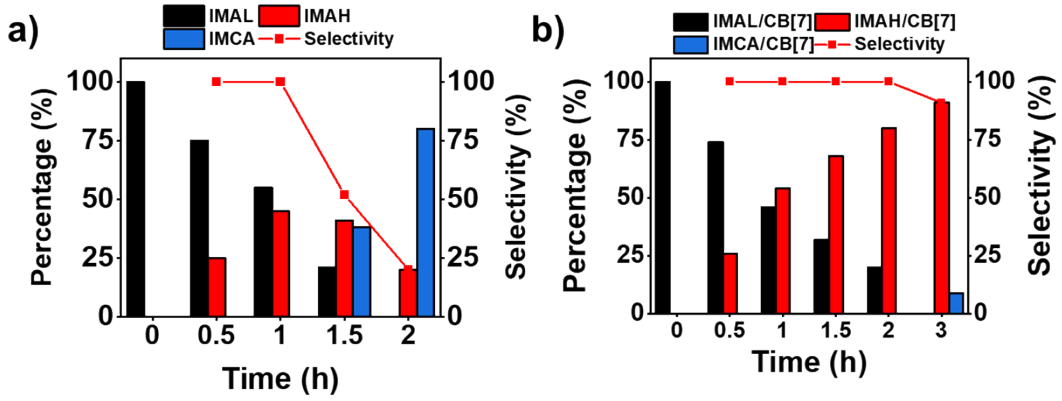

Figure S29. Kinetic profile of photo-induced oxidation of IMAL in pD 2.0 buffer in the absence or c) in the presence of CB[7].

12. Photo-oxidation product analysis

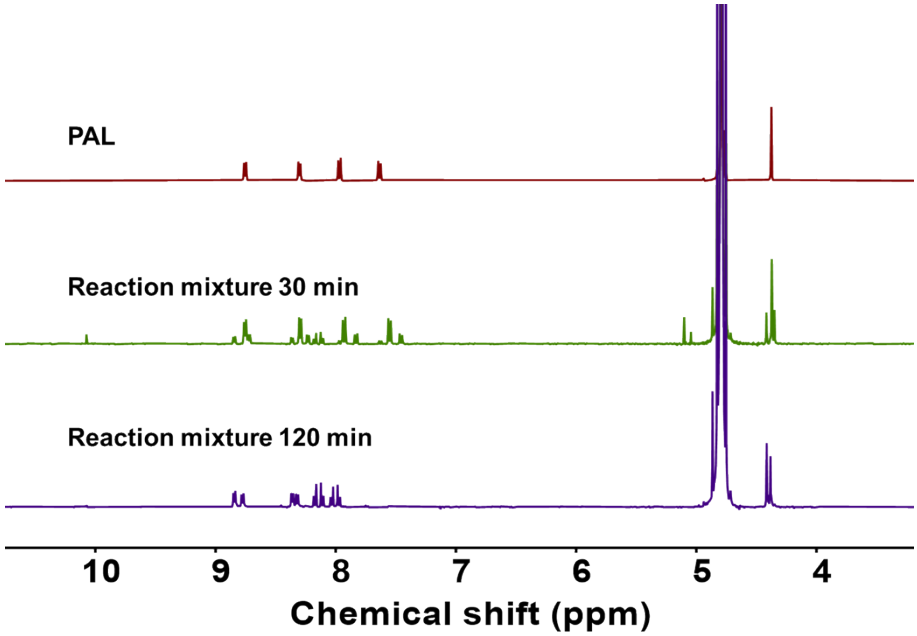

Figure S30. ^{1}H NMR spectra of compound PAL, reaction mixture after irradiating for 30 min, and 120 min.

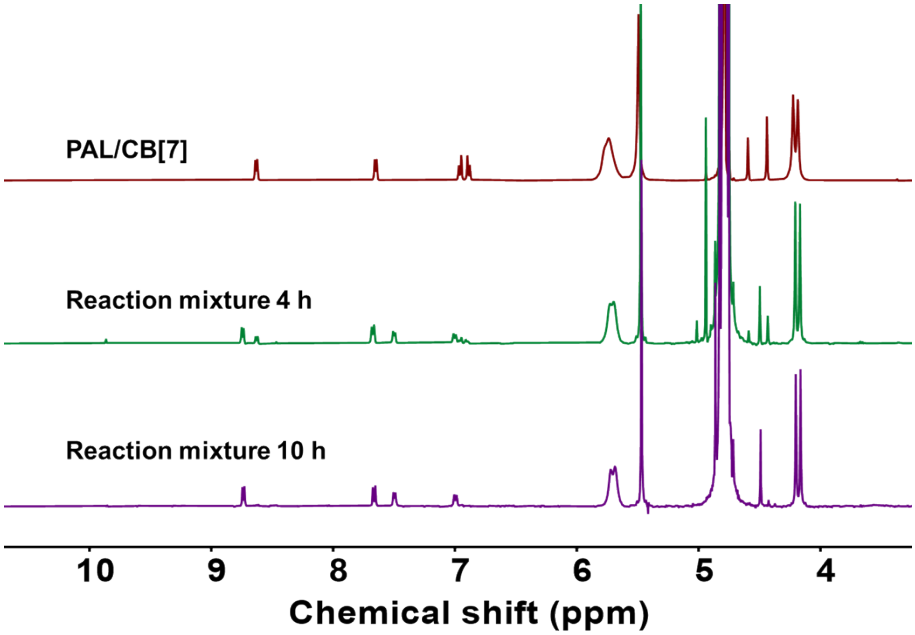

Figure S31. ^{1}H NMR spectra of the host-guest complex PAL/CB[7], reaction mixture after irradiating for 4 hours, and 10 hours.

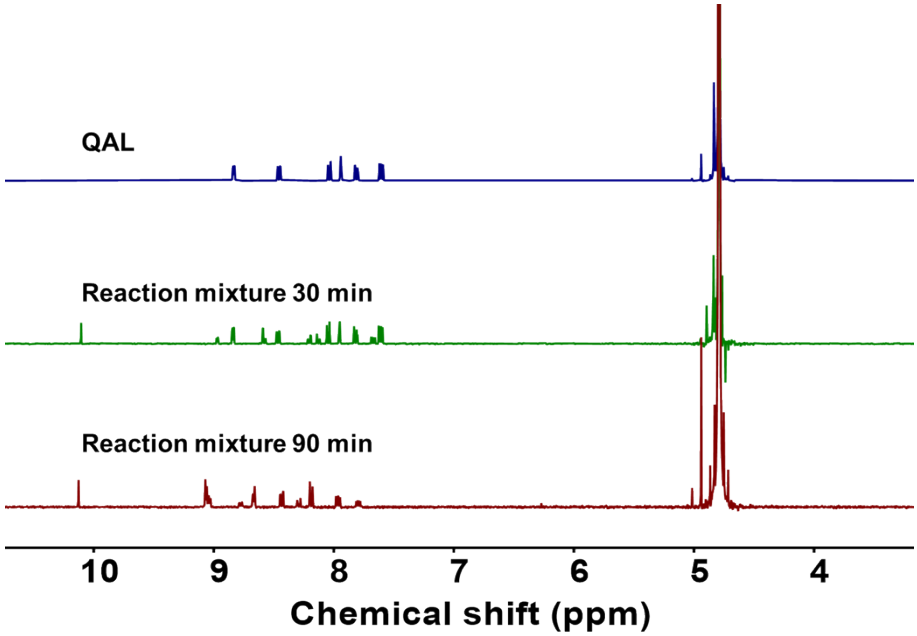

Figure S32. ^{1}H NMR spectra of compound QAL, reaction mixture after irradiating for 30 min, and 90 min.

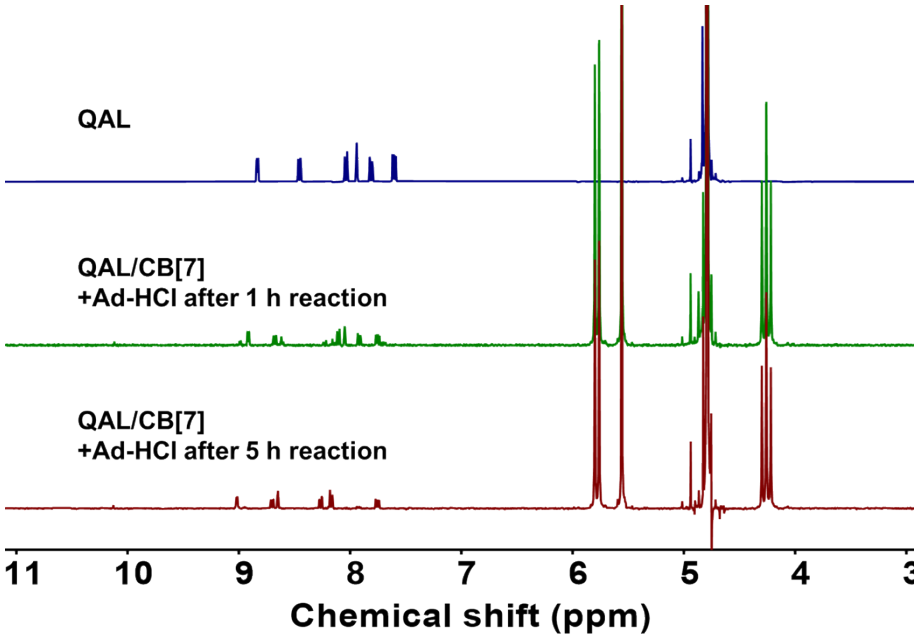

Figure S33. ^{1}H NMR spectra of compound QAL, reaction mixture of QAL/CB[7] after irradiating for 1 h, and 5 h.

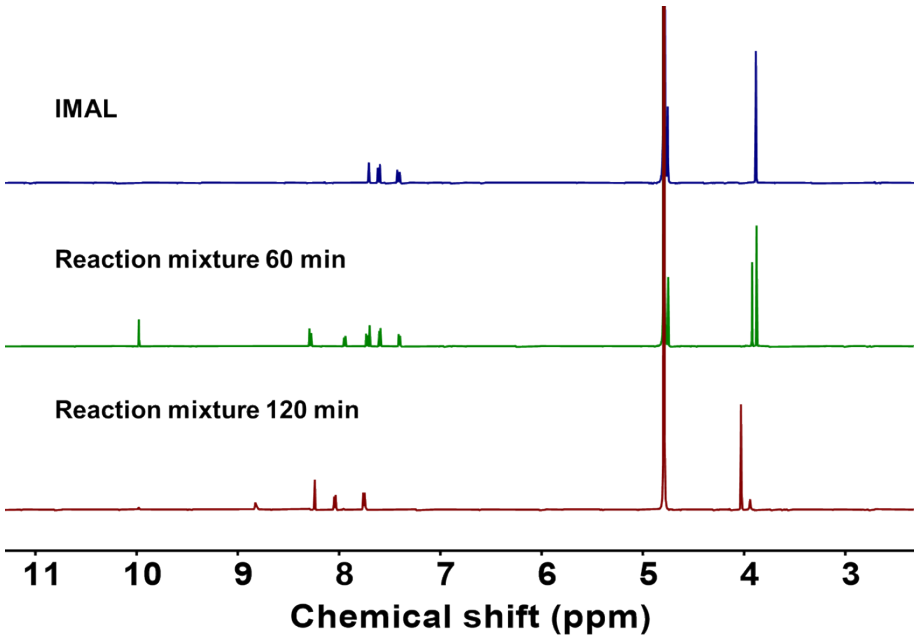

Figure S34. ^{1}H NMR spectra of compound IMAL, reaction mixture after irradiating for 60 min, and 120 min.

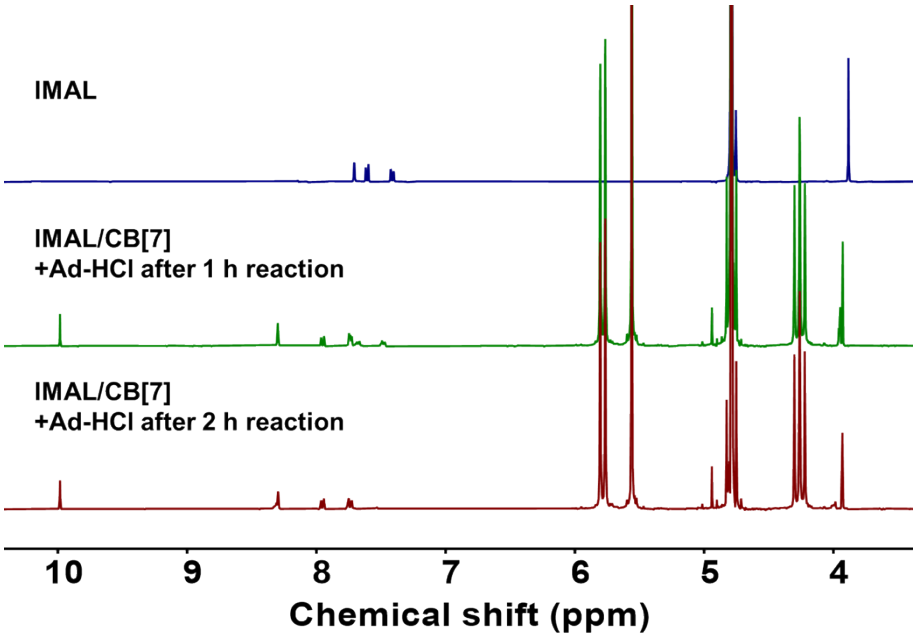

Figure S35. ^{1}H NMR spectra of compound IMAL, reaction mixture of IMAL/CB[7] after irradiating for 60 min, and 120 min.

13. Measurement of pKa

The temperature was maintained to 25 ± 1 ℃, 1.0 mM PCA and PCA/CB[7] in 3.0 mL

H_2O were titrated by 100 mM NaOH in aqueous. The corresponding pKa values were derived by fitting the titration curves using the least-square regression.
The acid-base equilibrium is expressed by the following equation:

$$V_B = V_A \frac{C_A\alpha - [H^+] + [OH^-]}{C_B + [H^+] - [OH^-]}$$

where

$$\alpha = \frac{K_a}{[H^+] + K_a}$$

V_A is the total volume of the weak acid and V_B is the volume of strong base used during the titration. Respectively. K_a represents the acid dissociation constant. C_A and C_B are the concentrations of acid (titrate) and base (titrant), respectively. A is the fraction of conjugate base.

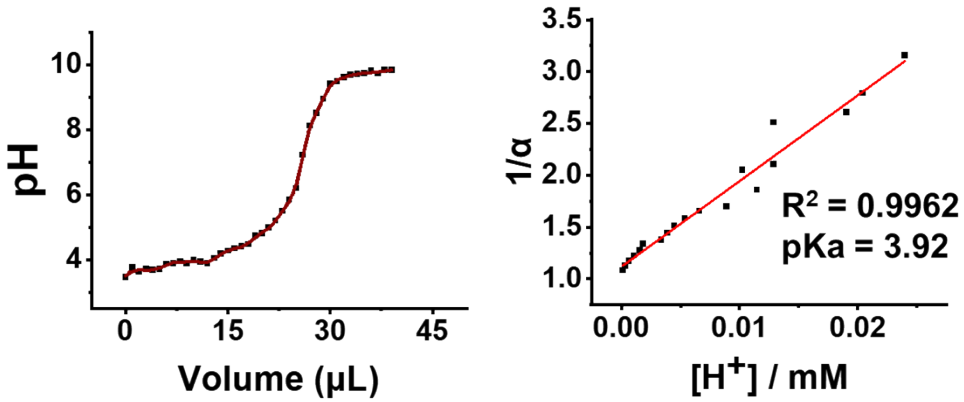

Figure S36. The titration curve and the calculation of pKa of PCA.

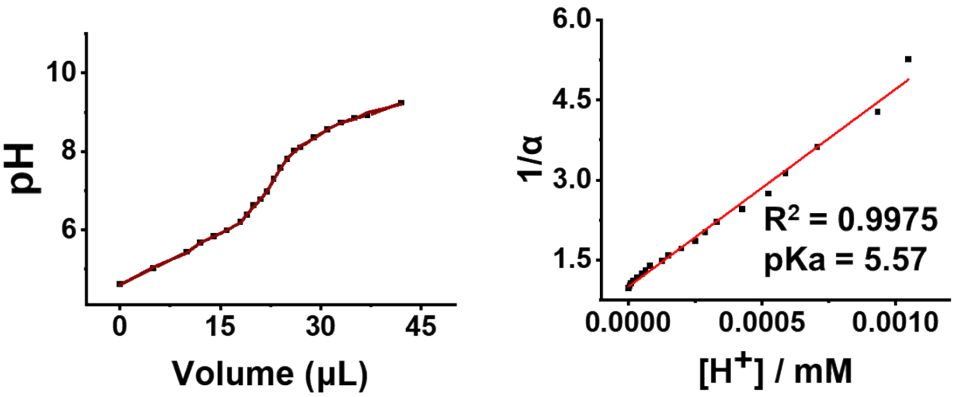

Figure S37. The titration curve and the calculation of pKa of PCA/CB[7].

14. ITC

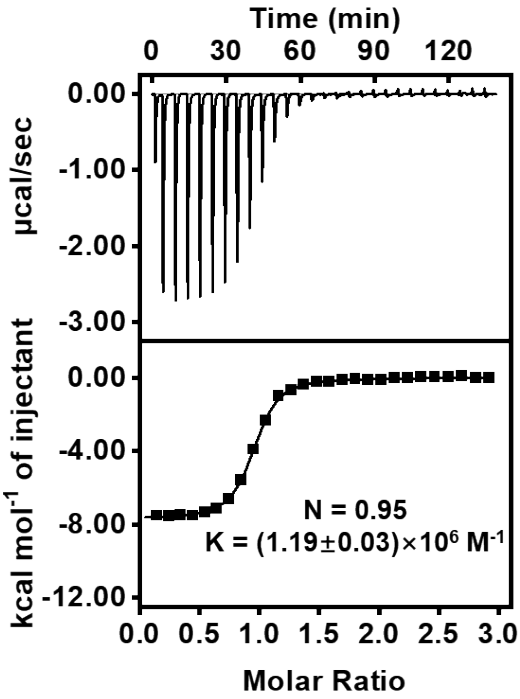

Figure S38. ITC data of 1.0 mM CB[7] adding to 0.10 mM PAL in 20 mM phosphate buffer (pH = 2.0).

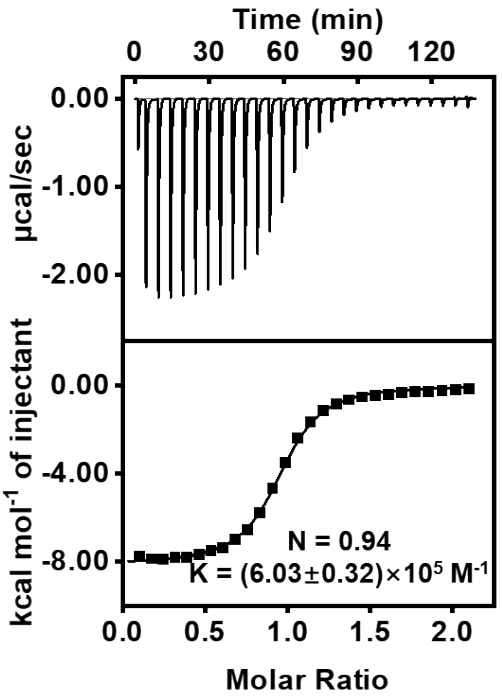

Figure S39. ITC data of 1.0 mM CB[7] adding to 0.10 mM PAL in 20 mM phosphate buffer (pH = 10.3).

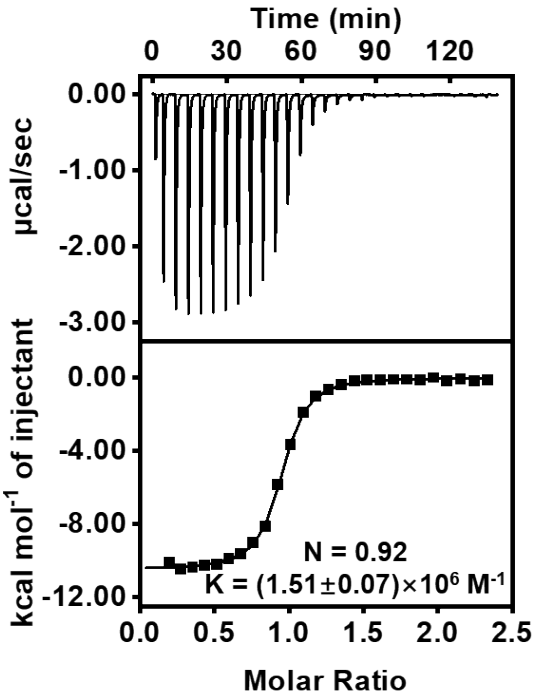

Figure S40. ITC data of 1.0 mM CB[7] adding to 0.10 mM PAH in 20 mM phosphate buffer (pH = 7.4).

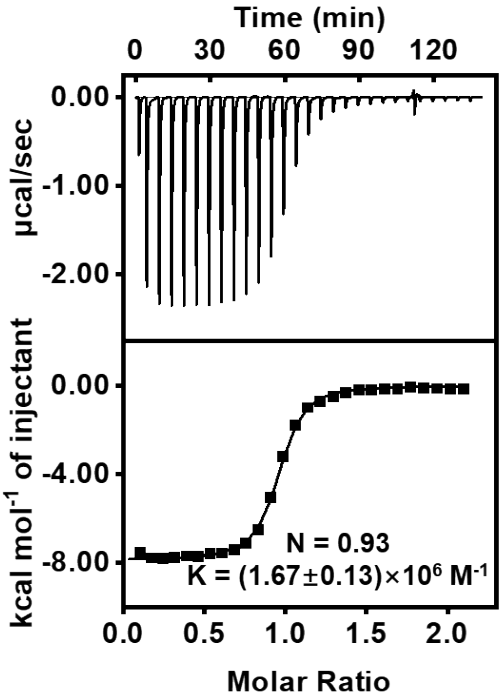

Figure S41. ITC data of 1.0 mM CB[7] adding to 0.10 mM PAH in 20 mM phosphate buffer (pH = 2.0).

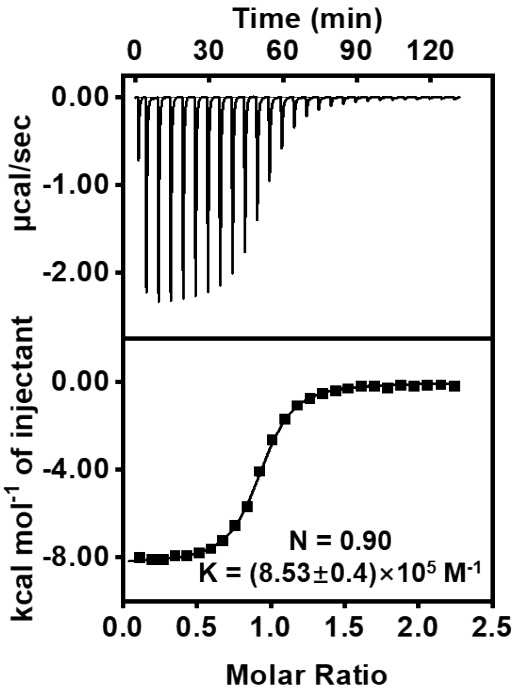

Figure S42. ITC data of 1.0 mM CB[7] adding to 0.10 mM PAH in 20 mM phosphate buffer (pH = 10.3).

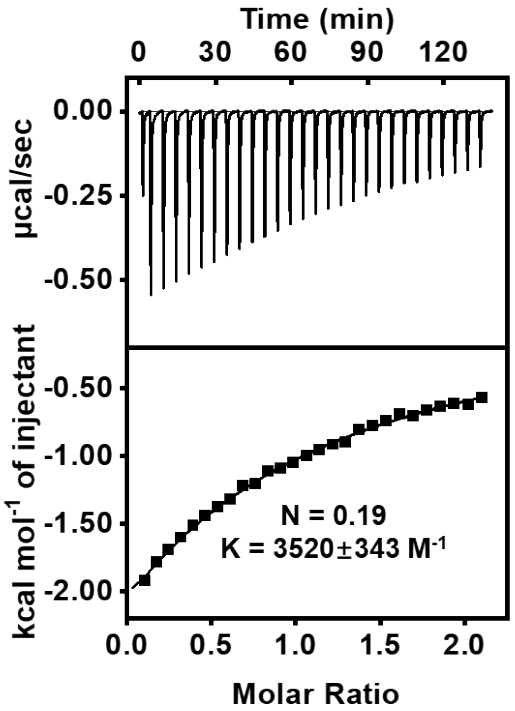

Figure S43. ITC data of 1.0 mM CB[7] adding to 0.10 mM PCA in 20 mM phosphate buffer (pH = 7.4).

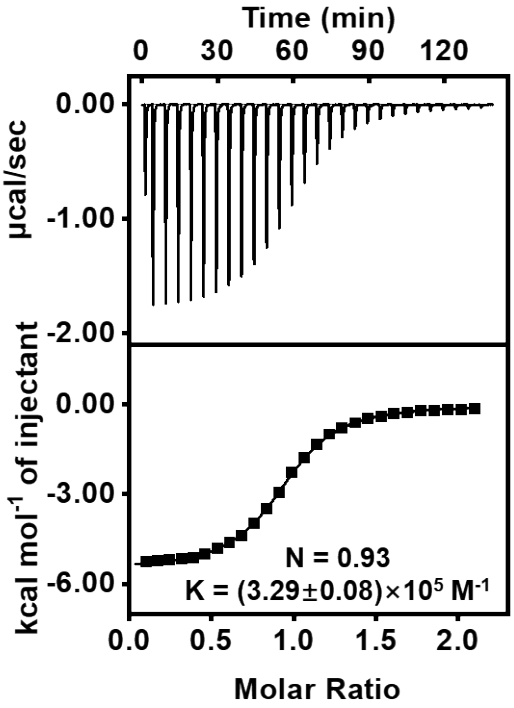

Figure S44. ITC data of 1.0 mM CB[7] adding to 0.10 mM PCA in 20 mM phosphate buffer (pH = 2.0).

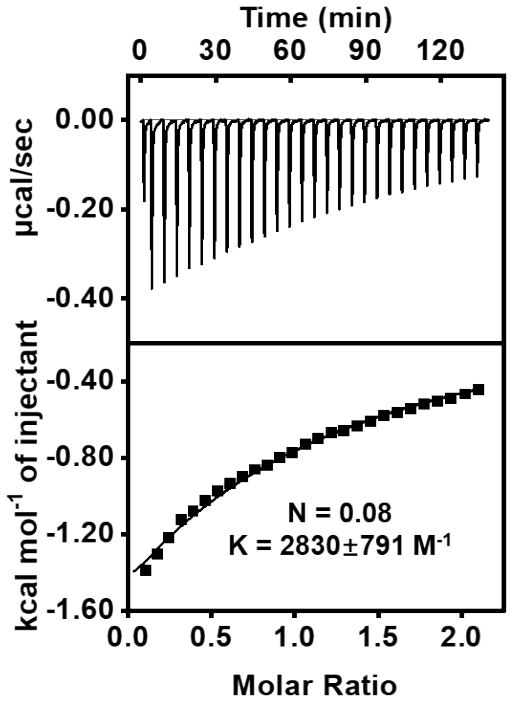

Figure S45. ITC data of 1.0 mM CB[7] adding to 0.10 mM PAL in 20 mM phosphate buffer (pH = 10.3).

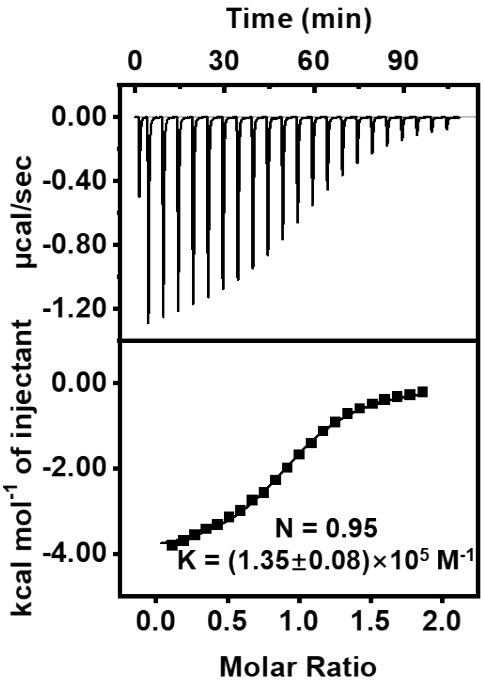

Figure S46. ITC data of 1.0 mM CB[7] adding to 0.10 mM QAL in 20 mM phosphate buffer (pH = 2.0).

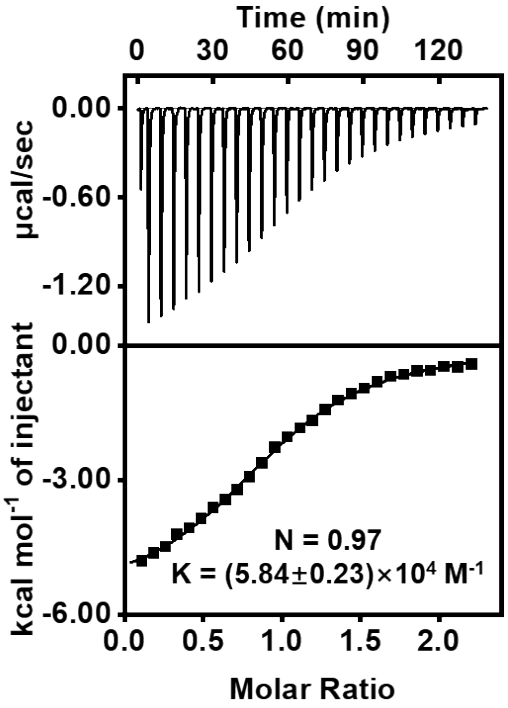

Figure S47. ITC data of 1.0 mM CB[7] adding to 0.10 mM IMAL in 20 mM phosphate buffer (pH = 2.0).

15. Discussion on the impact of binding thermodynamics on the reaction

We have revealed that the reactivity of ketyl radical and benzoyl radical can be modulated by the host-guest interaction of CB[7], resulting in the selective formation of aldehyde. We also wondered whether the binding thermodynamics between CB[7] and substrate/products can be another possible reason. To answer this question, ITC experiments were carried out to study the binding thermodynamics of PAL/CB[7], PAH/CB[7], and PCA/CB[7]. As shown in Table S1, under the neutral condition of pH 7.4, PCA indeed showed a relatively low binding affinity to CB[7] because of the electrostatic repulsion between the negative charged carboxylic group of PCA and the carbonyl portal. However, under pH 2.0, a condition in which PCA was fully protonated (see Figure S36 and S37 for details), the difference among the binding constants of PAL/CB[7], PAH/CB[7], PCA/CB[7] was negligible. Notably, as indicated by the photo induced oxidation reaction carried out in the acid buffer of pD 2.0, a high aldehyde yield of 86% with selectivity of 91% could also be realized (Table S1 and Figure S17). Therefore, these results indicate that binding thermodynamics only has little influence on the enhanced aldehyde selectivity, and the host-guest interaction is mainly responsible for the modulation on the reactivity of radical intermediates.

	lg(K) of PAL/CB[7]	lg(K) of PAH/CB[7]	lg(K) of PCA/CB[7]	Yield of PAH	Selectivity of PAH
pH = 7.4	6.04	6.18	3.55	91%	95%
pH = 2.0	6.08	6.22	5.51	86%	91%

Table S1. The binding constants of PAL/CB[7], PAH/CB[7], PCA/CB[7], the yield and selectivity of PAH/CB[7] obtained in pH 2.0 and pH 7.4 buffers. The reaction time is 10 h.

16. Theoretical calculation

All Density Functional Theory (DFT) calculations were conducted employing the Gaussian 16 program.[2] In each DFT calculation, the SMD solvation model was applied.[3] The optimized geometry and frequency calculations were calculated using the UB3LYP/6-31+g(d,p) level of theory with Grimme's D3 dispersion correction.[4-8] These optimizations were performed without imposing any constraints on the molecular geometry, and the default convergence criteria provided by Gaussian 16 were employed. There are no imaginary frequencies for optimized structure. One-electron energies of singly occupied molecular orbitals and Mulliken spin densities radical cation were calculated. The electronic energies calculated by unrestricted DFT are listed in Table S2, S3. The SOMO energies in Fig 3b and Fig 4b refer to α-HOMO energies.

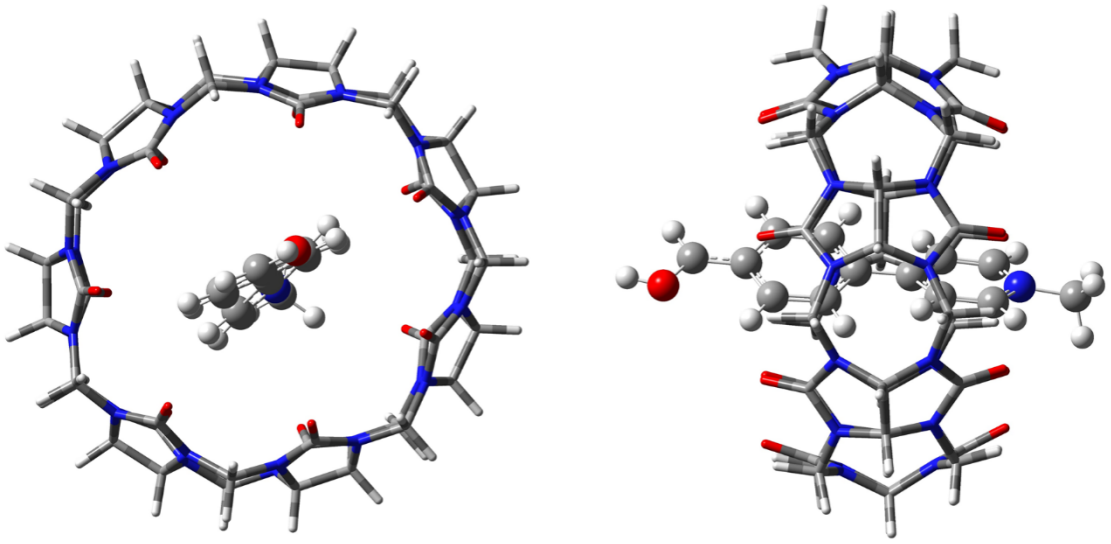

Figure S48. The top and side views of the optimized structure of ketyl radical/CB[7].

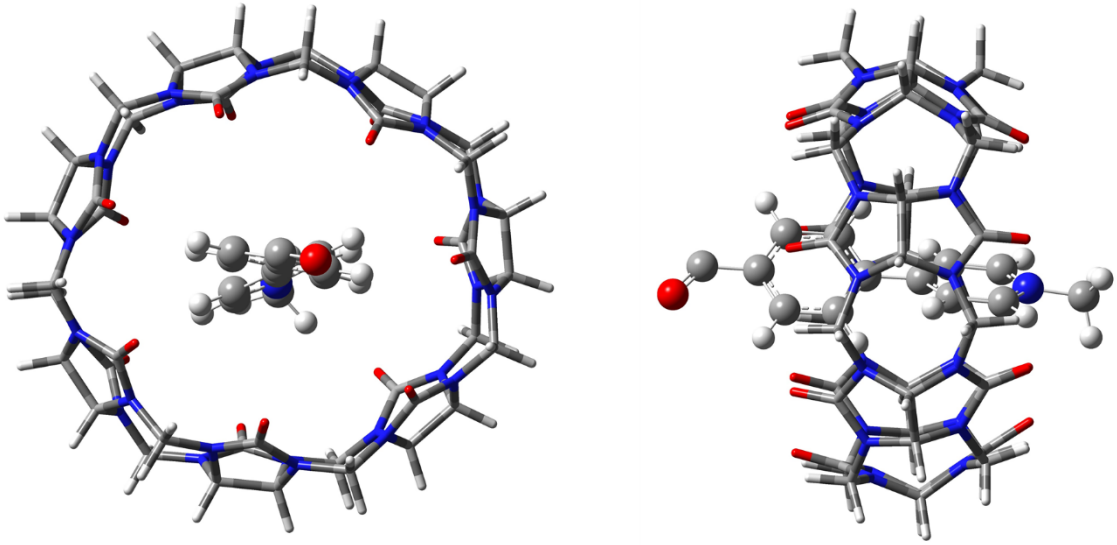

Figure S49. The top and side views of the optimized structure of benzoyl radical/CB[7].

Ketyl radical	α (eV)	β (eV)	Ketyl radical/CB[7]	α (eV)	β (eV)
LUMO+2	-0.43	-1.12	LUMO+2	-2.57	-2.59
LUMO+1	-1.19	-1.48	LUMO+1	-2.65	-2.75
LUMO	-2.11	-2.98	LUMO	-3.47	-4.26
HOMO	-4.70	-7.02	HOMO	-5.91	-8.24
HOMO-1	-7.36	-7.25	HOMO-1	-8.51	-8.32
HOMO-2	-7.49	-7.99	HOMO-2	-8.62	-8.79

Table S2. The calculated electronic energies of ketyl radical and ketyl radical/CB[7].

Benzoyl radical	α (eV)	β (eV)	Benzoyl radical/CB[7]	α (eV)	β (eV)
LUMO+2	-1.38	-1.54	LUMO+2	-2.77	-2.71
LUMO+1	-1.70	-2.26	LUMO+1	-3.31	-3.32
LUMO	-2.93	-2.85	LUMO	-4.46	-4.44
HOMO	-5.89	-7.41	HOMO	-6.32	-8.61
HOMO-1	-7.44	-7.57	HOMO-1	-8.62	-8.64
HOMO-2	-7.56	-8.24	HOMO-2	-8.67	-8.96

Table S3. The calculated electronic energies of benzoyl radical and benzoyl radical/CB[7].

	Spin density
Ketyl radical	0.49
Ketyl radical/CB[7]	0.48
Benzoyl radical	0.91
Benzoyl radical/CB[7]	0.73

Table S4. The calculated spin densities of benzyl carbon atoms in ketyl radical, ketyl radical/CB[7], benzoyl radical and benzoyl radical/CB[7].

17. References

(1) Kim, J.; Jung, I.-S.; Kim, S.-Y.; Lee, E.; Kang, J.-K.; Sakamoto, S.; Yamaguchi, K.; Kim, K. New Cucurbituril Homologues: Syntheses, Isolation, Characterization, and X-ray Crystal Structures of Cucurbit[n]uril (n = 5, 7, and 8). *J. Am. Chem. Soc.* **2000**, *122*, 540-541.
(2) Gaussian 16 Rev. C.01; Wallingford, CT, 2016. https://gaussian.com/gaussian16 (accessed. 2016)
(3) Marenich, A. V.; Cramer, C. J.; Truhlar, D. G. Universal Solvation Model Based on Solute Electron Density and on a Continuum Model of the Solvent Defined by the Bulk Dielectric Constant and Atomic Surface Tensions. *J. Phys. Chem. B* **2009**, *113*, 6378-6396.
(4) Stephens, P. J.; Devlin, F. J.; Chabalowski, C. F.; Frisch, M. J. Ab Initio Calculation of Vibrational Absorption and Circular Dichroism Spectra Using Density Functional Force Fields. *J. Phys. Chem.* **1994**, *98*, 11623-11627.
(5) Becke, A. D. Density-functional thermochemistry. III. The role of exact exchange. *J. Chem. Phys.* **1993**, *98*, 5648-5652.
(6) Hehre, W. J.; Ditchfield, R.; Pople, J. A. Self—Consistent Molecular Orbital Methods. XII. Further Extensions of Gaussian—Type Basis Sets for Use in Molecular Orbital Studies of Organic Molecules. *J. Chem. Phys.* **2003**, *56*, 2257-2261.
(7) McLean, A. D.; Chandler, G. S. Contracted Gaussian basis sets for molecular calculations. I. Second row atoms, Z=11–18. *J. Chem. Phys.* **2008**, *72*, 5639-5648.
(8) Grimme, S.; Antony, J.; Ehrlich, S.; Krieg, H. A consistent and accurate ab initio parametrization of density functional dispersion correction (DFT-D) for the 94 elements H-Pu. *J. Chem. Phys.* **2010**, *132*, 154104.